doi:10.1093/brain/awv305 BRAIN 2016: 139; 193–203 | 193

BRAIN
A JOURNAL OF NEUROLOGY

Preclinical properties and human *in vivo* assessment of ^{123}I-ABC577 as a novel SPECT agent for imaging amyloid-β

Yoshifumi Maya,[1] Yuki Okumura,[1] Ryohei Kobayashi,[1] Takako Onishi,[1] Yoshinari Shoyama,[1] Olivier Barret,[2] David Alagille,[2] Danna Jennings,[2] Kenneth Marek,[2] John Seibyl,[2] Gilles Tamagnan,[2] Akihiro Tanaka[1] and Yoshifumi Shirakami[1]

Non-invasive imaging of amyloid-β in the brain, a hallmark of Alzheimer's disease, may support earlier and more accurate diagnosis of the disease. In this study, we assessed the novel single photon emission computed tomography tracer ^{123}I-ABC577 as a potential imaging biomarker for amyloid-β in the brain. The radio-iodinated imidazopyridine derivative ^{123}I-ABC577 was designed as a candidate for a novel amyloid-β imaging agent. The binding affinity of ^{123}I-ABC577 for amyloid-β was evaluated by saturation binding assay and *in vitro* autoradiography using post-mortem Alzheimer's disease brain tissue. Biodistribution experiments using normal rats were performed to evaluate the biokinetics of ^{123}I-ABC577. Furthermore, to validate ^{123}I-ABC577 as a biomarker for Alzheimer's disease, we performed a clinical study to compare the brain uptake of ^{123}I-ABC577 in three patients with Alzheimer's disease and three healthy control subjects. ^{123}I-ABC577 binding was quantified by use of the standardized uptake value ratio, which was calculated for the cortex using the cerebellum as a reference region. Standardized uptake value ratio images were visually scored as positive or negative. As a result, ^{123}I-ABC577 showed high binding affinity for amyloid-β and desirable pharmacokinetics in the preclinical studies. In the clinical study, ^{123}I-ABC577 was an effective marker for discriminating patients with Alzheimer's disease from healthy control subjects based on visual images or the ratio of cortical-to-cerebellar binding. In patients with Alzheimer's disease, ^{123}I-ABC577 demonstrated clear retention in cortical regions known to accumulate amyloid, such as the frontal cortex, temporal cortex, and posterior cingulate. In contrast, less, more diffuse, and non-specific uptake without localization to these key regions was observed in healthy controls. At 150 min after injection, the cortical standardized uptake value ratio increased by ~60% in patients with Alzheimer's disease relative to healthy control subjects. Both healthy control subjects and patients with Alzheimer's disease showed minimal ^{123}I-ABC577 retention in the white matter. These observations indicate that ^{123}I-ABC577 may be a useful single photon emission computed tomography imaging maker to identify amyloid-β in the human brain. The availability of an amyloid-β tracer for single photon emission computed tomography might increase the accessibility of diagnostic imaging for Alzheimer's disease.

1 Research Centre, Nihon Medi-Physics Co., Ltd., Chiba, Japan
2 Molecular Neuroimaging, New Haven, CT, USA

Correspondence to: Yoshifumi Maya,
Research Centre, Nihon Medi-Physics Co., Ltd.
Kitasode 3-1, Sodegaura,
Chiba 299-0266,
Japan
E-mail: yoshifumi_maya@nmp.co.jp

Keywords: Alzheimer's disease; amyloid-β; imaging; single photon emission computed tomography; radiotracer

Abbreviations: PHF = paired helical filament; SPECT = single photon emission computed tomography; SUV(R) = standardized uptake value (ratio)

Received April 24, 2015. Revised August 11, 2015. Accepted August 28, 2015. Advance Access publication October 21, 2015

Introduction

Alzheimer's disease is a neurodegenerative disorder characterized by cognitive decline such as memory impairment, disorientation, and impaired language function (McKhann *et al.*, 2011). Senile plaques containing amyloid-β peptides and neurofibrillary tangles composed of hyperphosphorylated tau in the brain represent the neuropathological hallmarks of Alzheimer's disease (Braak and Braak, 1991). The cortical deposition of amyloid-β plaques is regarded as one of the earliest pathological markers in Alzheimer's disease (Aisen *et al.*, 2010; Bateman *et al.*, 2012; Villemagne *et al.*, 2013). In addition, amyloid-β plaques are believed to play a crucial role in the development of Alzheimer's disease (Hardy and Higgins, 1992; Roberson and Mucke, 2006; Sperling *et al.*, 2009; Huijbers *et al.*, 2015). Accordingly, various strategies aimed at preventing or reducing the accumulation of amyloid-β are underway to develop potential therapies for Alzheimer's disease (Reiman *et al.*, 2011; Schneider *et al.*, 2014; Sperling *et al.*, 2014). Therefore, amyloid-β imaging agents for PET or single photon emission computed tomography (SPECT) that can detect amyloid-β plaques *in vivo* may not only assist with the early and accurate diagnosis of Alzheimer's disease but may also play an important role in the development of anti-amyloid-β therapies by identifying subjects with amyloid-β plaques in the brain and monitoring their treatment response.

Over the past few years, three such amyloid-β imaging agents for PET [^{18}F-florbetapir (Choi *et al.*, 2009; Clark *et al.*, 2011), ^{18}F-flutemetamol (Nelissen *et al.*, 2009; Vandenberghe *et al.*, 2010), and ^{18}F-florbetaben (Rowe *et al.*, 2008; Barthel *et al.*, 2011)] have been approved by the United States Food and Drug Administration and the European Medicines Agency as radioactive diagnostic agents to estimate amyloid-β neuritic plaque density in adults being evaluated for Alzheimer's disease and dementia. On the other hand, there has been a lack of SPECT ligands available for the clinical diagnosis of Alzheimer's disease. In spite of the considerable effort to develop SPECT tracers (Kung *et al.*, 2003; Qu *et al.*, 2007; Ono *et al.*, 2013; Chen *et al.*, 2015), clinically useful amyloid-β imaging agents for SPECT have not been reported in humans.

It is well known that the resolution and sensitivity of SPECT are inferior to those of PET. However, there are more clinical imaging systems for SPECT installed in medical centres and community hospitals. Thus, if SPECT imaging tracers targeting amyloid-β plaques could be developed, this would increase the accessibility of diagnostic imaging for Alzheimer's disease. As such, the development of a SPECT imaging agent would benefit a large number of Alzheimer's disease patients. In this study, we designed and prepared a novel SPECT imaging agent, ^{123}I-ABC577, and examined its preclinical properties. In addition, we performed the first clinical study to assess the safety and efficacy of ^{123}I-ABC577 in humans.

Materials and methods

All reagents were commercial products and used without further purification unless otherwise indicated. Post-mortem human samples from four patients with Alzheimer's disease (86-year-old female, frontal lobe; 87-year-old female, frontal lobe; 79-year-old male, frontal lobe; and 73-year-old male, hippocampus) and one control subject (44-year-old female, frontal lobe) were acquired from Analytical Biological Services Inc. The presence of amyloid-β plaques and paired helical filament (PHF)-tau was examined by immunohistochemical staining using the anti-amyloid-β monoclonal antibody 82E1 (Immuno-Biological Laboratories Co., Ltd) and anti-PHF-tau monoclonal antibody AT8 (Innogenetics). Optical microscopy images were acquired using a Keyence BZ-9000 microscope (Keyence Corporation). Wistar rats were purchased from Japan SLC, Inc., housed in conditions of controlled temperature (18–28°C) and lighting (12:12 h light–dark cycle), and given free access to food and water. The protocols for the animal experiments were approved by the committee on animal welfare at Nihon Medi-Physics Co., Ltd.

Chemistry and radiochemistry

The tributyltin precursor of ^{123}I-ABC577 and the reference standard (ABC577) were custom-synthesized by the Nard Institute, Ltd. No-carrier-added radio-iodinated ^{123}I-ABC577 was successfully prepared through an iododestannylation reaction from the corresponding tributyltin precursor (Fig. 1). Details are provided in the online Supplementary material. Briefly, to initiate the reaction, the precursor solution was added to a mixture of sodium ^{123}I-iodide, hydrogen peroxide, and hydrochloric acid in a sealed vial. After the reaction was allowed to proceed at 40°C for 10 min, the radio-iodinated ligand was purified by high-performance liquid chromatography. ^{123}I-ABC577 was obtained in 3–57% radiochemical yields, with radiochemical purities >94% and specific activities >100 GBq/μmol.

Saturation binding assay

Frontal lobe grey matter containing abundant amyloid-β plaques but minimal PHF-tau was carefully separated from white matter in the cortical tissue. Homogenates were then prepared with a tissue homogenizer in phosphate-buffered saline (PBS). Tissue homogenates were frozen at −80°C until used for binding assays. The reaction mixture contained 50 μl of tissue homogenates (25 μg) and 100 μl of ^{123}I-ABC577 (final concentration, 0.2–25 nM) in a final volume of 250 μl. Non-specific binding was defined in the presence of 1 μM Pittsburgh compound B. The mixture was incubated at 22°C for 3 h, and the bound and the free radioactivity were separated by filtration under reduced pressure (MultiScreen HTS Vacuum Manifold; Merck Millipore), followed by three washes with PBS containing 0.1% bovine serum albumin. The radioactivity retained on the filters was counted in a gamma counter (ARC-7001; Hitachi Aloka Medical, Ltd.). The binding data were evaluated by fitting the data to a one-site binding model using GraphPad Prism (GraphPad Software, Inc.) through

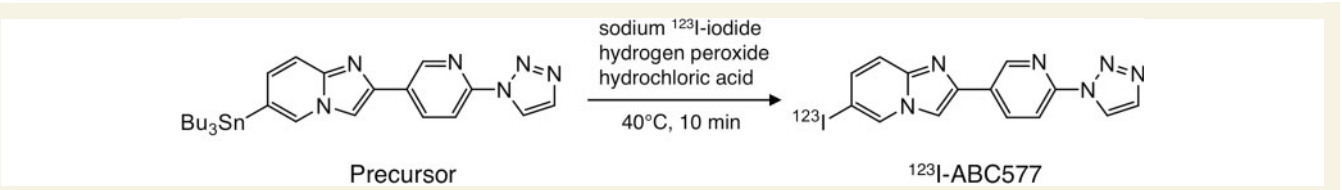

Figure 1 Radiosynthesis of ^{123}I-ABC577.

which the equilibrium dissociation constant (K_d) and maximum number of binding sites (B_{max}) were calculated.

In vitro autoradiography

Frozen brains from a control subject and four patients with Alzheimer's disease were cut into 5-μm sections with a cryostat (Leica Microsystems). Brain sections were dipped in PBS for 15 min, 5 min, and 5 min, and then dipped in PBS containing 1% bovine serum albumin. The sections were then incubated with ^{123}I-ABC577 (10 kBq/ml) for 30 min at room temperature. The sections were washed with PBS containing 1% bovine serum albumin for 5 min, followed by two 5-min rinses with PBS. Non-specific binding was determined in the presence of 5 μM ABC577. After drying, the ^{123}I-labelled sections were exposed to imaging plates (Fujifilm) overnight. The autoradiographic images were obtained using a BAS-2500 imaging instrument (Fujifilm) or Typhoon FLA7000 IP System (GE healthcare). Adjacent sections were immunostained using the anti-amyloid-β monoclonal antibody 82E1 and anti-PHF-tau monoclonal antibody AT8.

Selectivity screening

Pharmacological screening assays were conducted by Sekisui Medical Co., Ltd. The inhibitory effect of 10 μM ABC577 was evaluated in competition binding experiments against a panel of 91 types of receptors, ion channels, and transporters. Percentage inhibition ratios were calculated.

In vivo biodistribution in normal rats

A total of 21 male Wistar rats (129–142 g) that received iodine pretreatment were injected in the tail vein with ^{123}I-ABC577 (4 MBq). The rats were sacrificed at 5 min, 30 min, 1 h, 3 h, 6 h, 14 h, and 24 h post-injection (three animals at each time point). The organs of interest were removed and weighed, and the radioactivity was measured with a single channel analyser (Ohyo Koken Kogyo Co., Ltd.). The per cent dose per gram of tissue (%ID/g) was calculated by comparing the tissue counts with the count of the initial dose.

SPECT study

All study procedures were conducted at the Institute for Neurodegenerative Disorders and Molecular NeuroImaging in New Haven, CT. This study was approved by the New England Institutional Review Board and the United States Food and Drug Administration. Written informed consent was obtained from all subjects and caregivers (for the probable Alzheimer's disease patients) prior to study entry and any protocol-specific procedures.

Participants

Three young and healthy controls (mean age: 24.5 years) and three patients with probable Alzheimer's disease (mean age: 66.8 years) were included in the study (Table 1). Alzheimer's disease patients were selected from an existing database and from referrals to Molecular NeuroImaging. Healthy controls were recruited from caregivers and a Molecular NeuroImaging database of healthy control participants. To qualify for participation, patients with Alzheimer's disease were required to be older than 50 years and to have met the National Institute of Neurological and Communicative Disorders and Stroke/Alzheimer's Disease and Related Disorders Association NINCDS/ADRDA criteria for probable Alzheimer's disease. In addition, participants were required to have met the Diagnostic and Statistical Manual of Mental Disorders, fourth edition, text revision criteria for dementia of Alzheimer's type, with a clinical dementia rating (CDR) score of 0.5, 1, or 2. All patients with Alzheimer's disease underwent the ^{18}F-florbetapir (Amyvid^{TM}; Eli lily and Co.) PET scan and showed moderate-to-frequent amyloid-β plaques based on visual interpretation. A detailed description of the ^{18}F-florbetapir PET procedure and image analysis is provided in the Supplementary material. Healthy controls were required to be male, between 20 and 30 years of age, and exhibit no signs of cognitive impairment as indicated by a CDR score of 0 and a score $\geqslant$28 on the Mini-Mental State Examination (MMSE). Additionally, participants with more than one first-degree relative with a diagnosis of Alzheimer's disease were excluded from participation as a healthy control. Subjects who showed evidence of any other significant neurodegenerative disease, stroke, or generalized cerebrovascular disease upon clinical examination or MRI were excluded from the study. No subjects had any contraindications to MRI examination, unstable medical conditions, or history of exposure to any radiation $>$15 mSv/year.

MRI and SPECT procedures

Brain MRI scanning (both 3D T_1- and T_2-weighted images) was performed for screening and co-registration purposes to facilitate semi-quantification of SPECT findings. Subjects were pretreated with stable iodine to reduce thyroid uptake of iodo-123 approximately 30 min prior to ^{123}I-ABC577 injection. All subjects received a single dose of ~185 MBq (5 mCi) of ^{123}I-ABC577 as a slow intravenous bolus injection followed by a 10 ml saline flush. Serial dynamic SPECT projection data were acquired using a research-dedicated three-headed SPECT

Table 1 Demographics and neuropsychological results

Study ID	Age at imaging (years)	Gender	MMSE	CDR	^{18}F-florbetapir scan
HC01	26	Male	30	0	–
HC02	22	Male	30	0	–
HC03	25	Male	28	0	–
AD01	66	Female	25	0.5	Positive
AD02	67	Female	26	1	Positive
AD03	66	Male	15	1	Positive

CDR = clinical dementia rating score; MMSE = Mini-Mental State Examination.

system (PICKER PRISM 3000XP; Philips) fitted with low-energy, high-resolution fan-beam collimators. Imaging was performed on healthy controls during three 90-min sessions: 0–90 min (6 × 10 min, 2 × 15 min), 120–210 min (4 × 22.5 min), and 240–330 min (4 × 22.5 min) after ^{123}I-ABC577 injection. Alzheimer's disease patients were imaged for 90 min at 150–240 min (4 × 22.5 min) after injection with ^{123}I-ABC577. Projection data were acquired using a 20% symmetric photopeak window centred on 159 keV for a total of 120 raw projection images sampled every 3°. Projection data were reconstructed with an iterative reconstruction algorithm (four iterations, 20 subsets) using an ordered subset expectation maximization (OSEM) software package, with a standardized Butterworth filter. Attenuation was corrected with Chang's method using ellipses manually drawn on the SPECT images (linear attenuation coefficient $\mu = 0.11\ cm^{-1}$). Phantom projection data in which the amount of radioactivity was known were also acquired and reconstructed to calculate a calibration factor.

Metabolism analysis

Venous sampling was performed for measurement of ^{123}I-ABC577 metabolism in the plasma. An intravenous line was inserted into an upper extremity vein for venous sampling. Venous blood samples were collected at 5, 15, 30, 60, 120, 180, 240, and 300 min post-injection in the healthy controls and at 180, 210, and 240 min post-injection in the Alzheimer's disease patients. Plasma samples were processed by acetonitrile denaturation, treating 1 ml of plasma with 1 ml of acetonitrile. After vigorous mixing and centrifugation at 3000*g* for 10 min, the supernatant was transferred to an autosampler vial and injected into the high-performance liquid chromatography system equipped with a Phenomenex Luna C18(2) (10 × 250 mm) at a flow rate of 4 ml/min using a gamma detector (LabLogic Systems). The mobile phase consisted of a mixture of methanol/water with 0.2% of triethylamine in a 75/25, v/v ratio. Gamma chromatograms were analysed by integration of all radioactive peaks. The percentage of the parent compound was calculated by dividing the area under the peak representing the parent compound by the sum of the area of all radioactive peaks.

Image analysis

SPECT images were analysed with the FusionViewer software package (AZE, Ltd.). All SPECT images were merged with magnetic resonance images (T_1-weighted images). Volumes of interest were drawn on coregistered magnetic resonance images and transferred to the SPECT images. Volumes of interest were defined for the frontal cortex, parietal cortex, temporal cortex, occipital cortex, anterior cingulate, posterior cingulate, subcortical white matter, and cerebellum. Using the calibration factor calculated from the phantom projection data, the average radioactivity concentration within each volume of interest was determined. The standardized uptake value (SUV) was calculated for all regions by normalizing based on the body weight and the injected dose. These were then used to derive the SUV ratio (SUVR), which was referenced to the cerebellum. Time-activity curves were generated in SUV units (g/ml) and in SUVR units. Average SUVR values over 90 min (150–240 min for Alzheimer's disease patients and 120–210 min for healthy controls) in the aforementioned regions are reported. The unweighted mean cortical-to-cerebellar SUVR was calculated by combining the individual values for each of the cortical regions (Mintun *et al.*, 2006; Joshi *et al.*, 2012). Additionally, ^{123}I-ABC577 SPECT images were evaluated visually by an experienced nuclear medicine physician blind to subject diagnosis. Averaged SPECT images acquired over 150–240 min (patients with Alzheimer's disease) and 120–210 min (healthy control subjects) post-injection were assessed for overall image quality and pattern of radiotracer uptake with particular attention to cortical regions known to be involved with amyloid-β deposition in Alzheimer's disease (lateral temporal lobes, frontal cortex, cingulate cortex, parietal lobes, and precuneus). Images were scored as overall positive or negative for evidence of increased tracer uptake in these relevant cortical regions. Because of a camera issue, only two images were acquired for subject HC02 during the second imaging session. Therefore, only 45 min were used to calculate the 90 min average for this subject.

Results

Saturation binding assay

To evaluate the *in vitro* binding affinity of ^{123}I-ABC577 for amyloid-β plaques, a saturation binding experiment was performed. The results of the ^{123}I-ABC577 saturation binding assay for post-mortem Alzheimer's disease brain homogenates from the frontal cortex suggest that the binding is specific and saturable. The binding data were well-fitted to

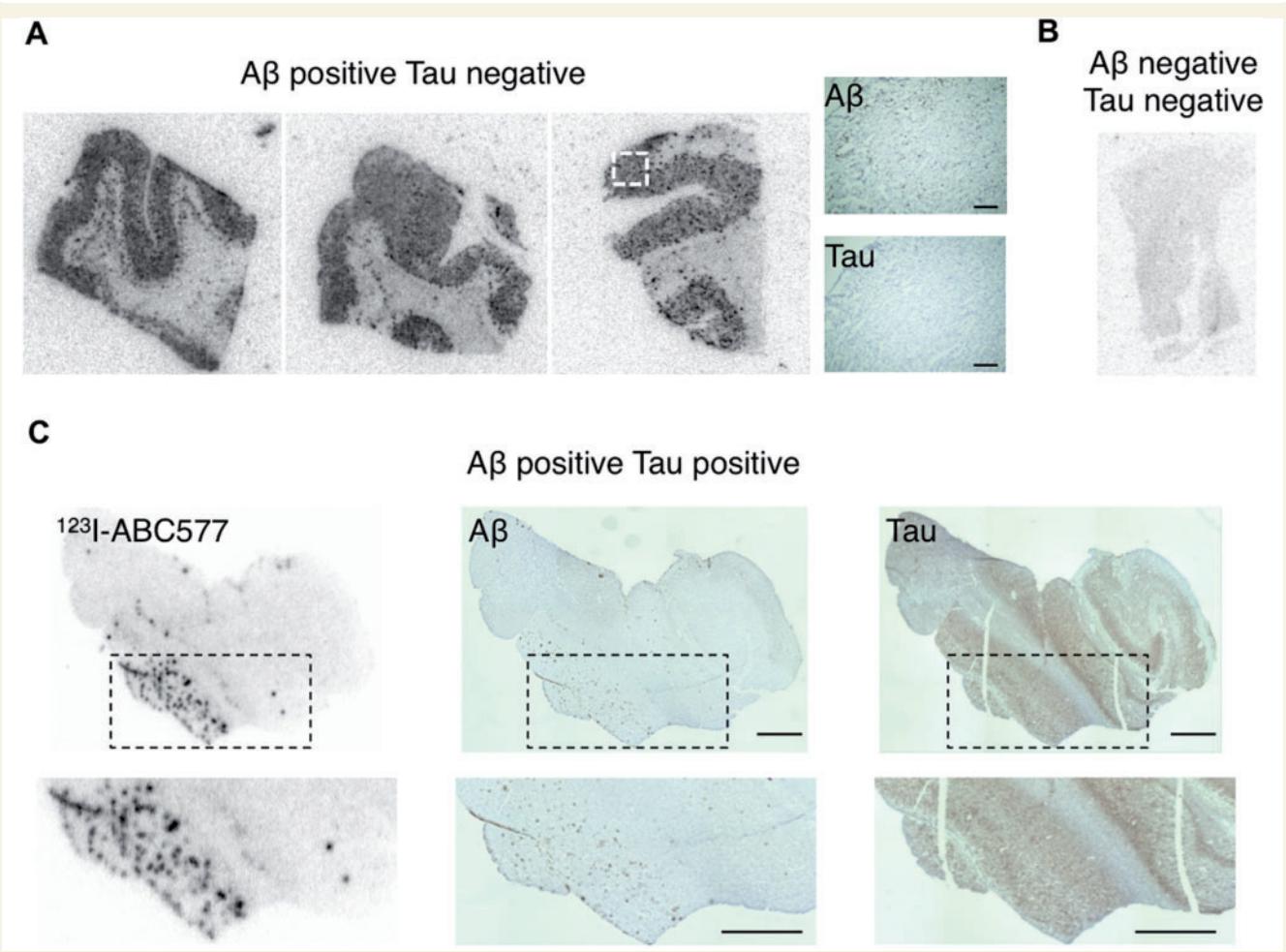

Figure 2 ***In vitro*** **autoradiograms of ^{123}I-ABC577 with different types of human brain sections.** (**A**) Distinct labelling was observed on Alzheimer's disease brain sections with abundant amyloid-β (Aβ) plaques but minimal PHF-tau. Immunostaining results in the area indicated by the white square are presented at a higher magnification. Scale bars = 0.5 mm. (**B**) Labelling was not observed on the control brain section. (**C**) Distribution of ^{123}I-ABC577-labeling co-localized with amyloid-β plaques but did not highlight PHF-tau pathology. (**C**, *top row*) Low magnification. (**C**, *bottom row*) High magnification from the framed areas. Scale bars = 2 mm.

a single binding site ($r^2 = 0.97$). The K_d estimated for ^{123}I-ABC577 was 1.83 nM, and B_{max} was 1235 fmol/mg tissue.

In vitro autoradiography

In vitro autoradiography to examine the ^{123}I-ABC577 binding profile was performed on 5 μm tissue sections from four patients with confirmed Alzheimer's disease and one control subject. When Alzheimer's disease brain sections from the frontal lobe containing abundant amyloid-β plaques but minimal PHF-tau were incubated with ^{123}I-ABC577, high-density labelling of ^{123}I-ABC577 compared to the control section was observed in the grey matter (site of amyloid-β deposition) (Fig. 2A and B). The labelling was completely blocked with an excessive concentration of ABC577, demonstrating specificity (data not shown). No difference was observed in the white matter free of amyloid-β pathology among the brain sections from Alzheimer's disease patients and the control subject. The tracer distribution coincided with anti-amyloid-β-antibody immune staining but not with anti-tau-antibody immune staining in the amyloid-β and tau-positive hippocampal brain section (Fig. 2C).

Selectivity screening

The selectivity of ABC577 binding was examined using assays consisting of 91 receptors, transporters, and ion channels. None of the receptors or transporters (e.g. dopamine transporter, serotonin receptors, GABA receptors, histamine receptors) was inhibited by more than 50% at 10-μM ABC577 concentrations (data not shown).

Biodistribution experiment

To assess the kinetic properties of ^{123}I-ABC577, biodistribution experiments were performed in normal rats. The biodistribution data are shown in Supplementary Table 1.

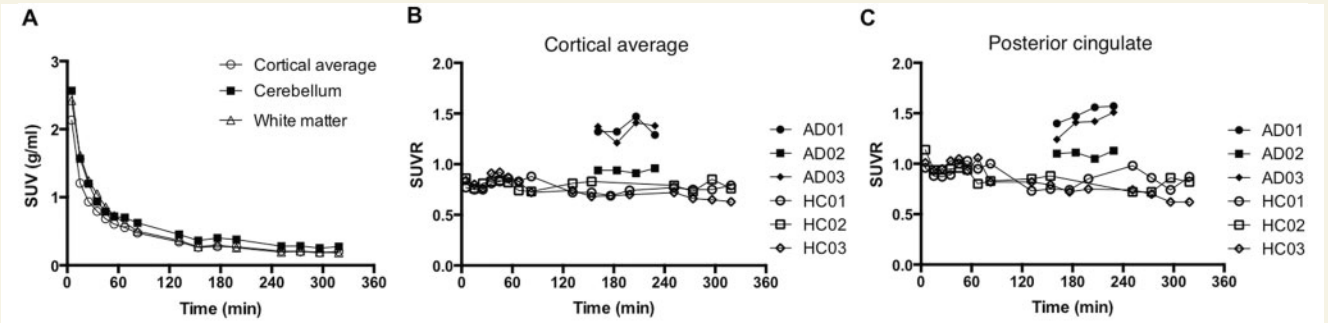

Figure 3 Time–activity curves for ^{123}I-ABC577. (**A**) Regional time-activity curves (SUV units) for healthy controls. Subjects were scanned for ~330 min. (**B** and **C**) Individual cortical-to-cerebellar SUVR time-activity curves for cortical average (**B**) and posterior cingulate (**C**) of healthy controls (0–330 min) and Alzheimer's disease patients (150–240 min).

Following its injection into the tail vein, ^{123}I-ABC577 showed rapid distribution and blood clearance, followed by urinary and hepatobiliary elimination. ^{123}I-ABC577 was distributed primarily to the liver, small intestine, kidneys, and adrenals. ^{123}I-ABC577 penetrated the blood–brain barrier, showing excellent brain uptake (0.788 %ID/g) at 5 min post-injection. In addition, ^{123}I-ABC577 displayed good clearance from the normal brain (0.044 %ID/g) at 60 min post-injection.

SPECT study

The experimental SPECT imaging agent ^{123}I-ABC577 for detecting amyloid-β plaques in the brain was evaluated in three healthy control subjects and three patients with Alzheimer's disease. ^{123}I-ABC577 was well tolerated in the population studied. No serious adverse events or clinically significant changes in laboratory or electrocardiogram parameters were observed.

Regional time—activity curves (SUV units) for ^{123}I-ABC577 in healthy controls are shown in Fig. 3A. Good brain penetration was observed, with a maximum SUV around 2.5 in all regions. The binding appeared to be reversible, with rapid washout from all areas including the white matter. On the basis of the healthy controls, Alzheimer's disease subjects were imaged for 90 min, from 150–240 min (4 × 22.5 min) post-injection, so that the SUVR was stable. Figure 3B and C show the individual SUVR time-activity curves for the cortical average and posterior cingulate in Alzheimer's disease patients (150–240 min) and healthy controls (0–330 min). A higher cortical-to-cerebellar SUVR in Patients AD01 and AD03 relative to the healthy controls was observed. Patient AD02 had a relatively low cortical-to-cerebellar SUVR compared to the other Alzheimer's disease subjects but showed an obviously high SUVR in the posterior cingulate at all time points. The SUVR showed only small changes during the scan for both healthy controls and Alzheimer's disease patients.

Analyses of metabolites assayed in the venous plasma demonstrated that ^{123}I-ABC577 was quickly metabolized, with ~10% of intact parent remaining at 60 min post-injection (Supplementary Fig. 1). There was no evidence of any differences between healthy controls and Alzheimer's disease patients; however, the samples from patients with Alzheimer's disease were only collected from 180 min post-injection, and the parent fraction levels were already very low (less than 5%) by this time. In all subjects, only one peak of radiometabolite, which is much more polar than the parent compound, was detected.

SPECT images of ^{123}I-ABC577 acquired over a 90-min period for healthy controls (120–210 min) and Alzheimer's disease patients (150–240 min) are shown in Fig. 4. Images were normalized to the uptake value in the cerebellum (units of SUVR) and displayed using the same colour scale range of 0.4–2.8. In Alzheimer's disease patients, ^{123}I-ABC577 uptake can be seen in cortical regions known to accumulate amyloid-β including the frontal cortex, parietal cortex, temporal cortex, and cingulate cortex. In Patients AD01 and AD03, focal areas of tracer retention were observed in the posterior cingulate, precuneus, temporal cortex, and parietal cortex. Patient AD02 showed a relatively low level of tracer retention compared to the other Alzheimer's disease subjects in the posterior cingulate, precuneus, and parietal cortex. In contrast, the healthy controls demonstrated homogeneously low non-specific binding without localization to these key regions. The white matter binding was visually low in subcortical regions in both healthy controls and patients with Alzheimer's disease. Blinded reading of the SUVR images correctly distinguished patients with Alzheimer's disease from healthy controls in all cases. SPECT images of different scan lengths demonstrated that scans as short as 22.5–45 min were sufficient to reliably distinguish ^{123}I-ABC577 uptake in Alzheimer's disease patients from that of healthy controls (Fig. 5).

Average SUVR values for over 90 min of acquisitions with ^{123}I-ABC577 are reported in Table 2. In the cortical regions, there were SUVR increases of ~20–70% in the

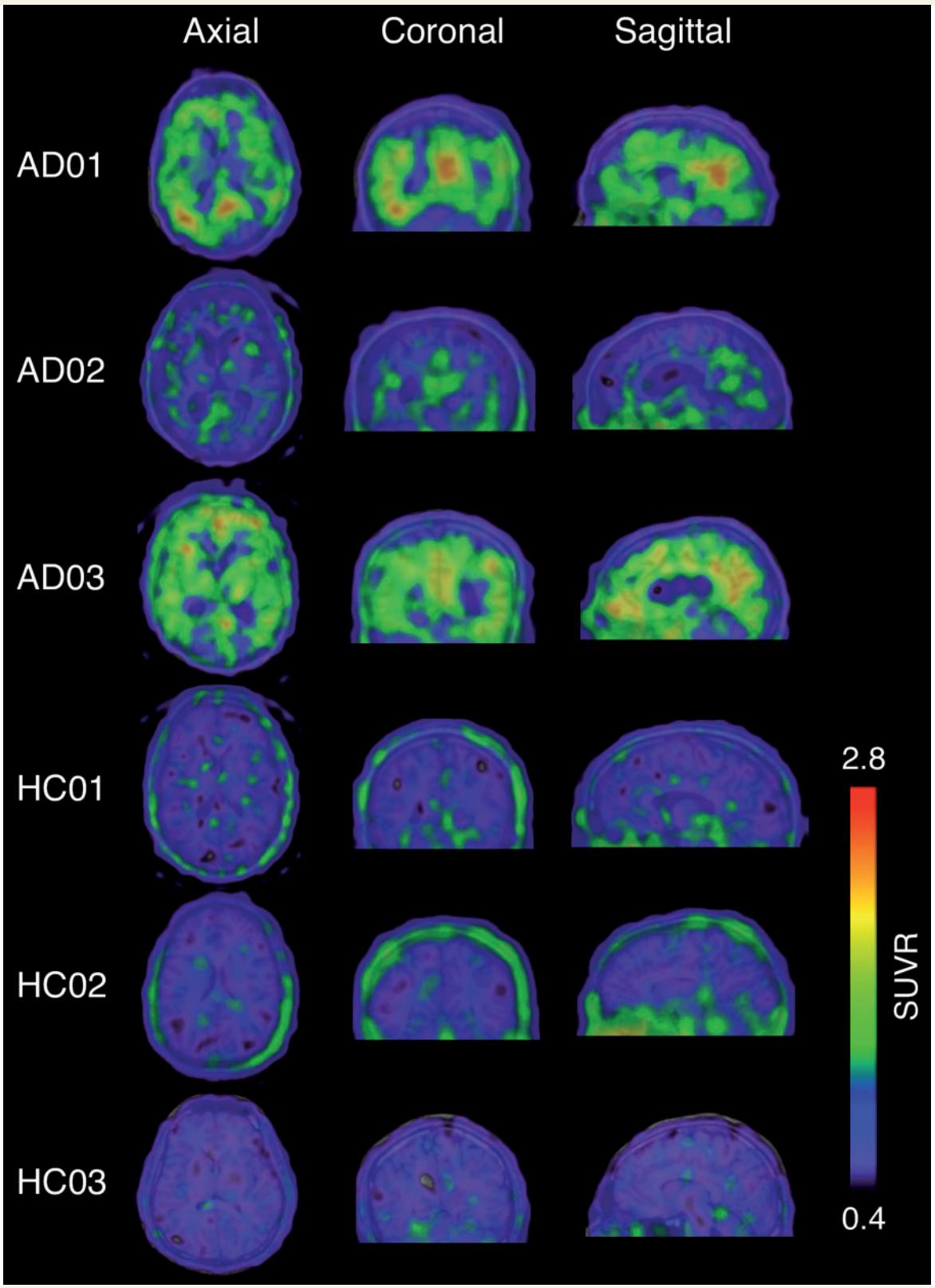

Figure 4 SPECT images of ^{123}I-ABC577. SUVR images over 90 min of acquisition in three healthy controls and three Alzheimer's disease patients. SPECT images are overlaid on individual coregistered magnetic resonance images. Axial views include the frontal lobe, anterior cingulate, posterior cingulate, insula, striatum, and lateral temporal lobe. Coronal views include the temporal lobe and posterior cingulate. Sagittal views include the anterior cingulate, posterior cingulate, and precuneus.

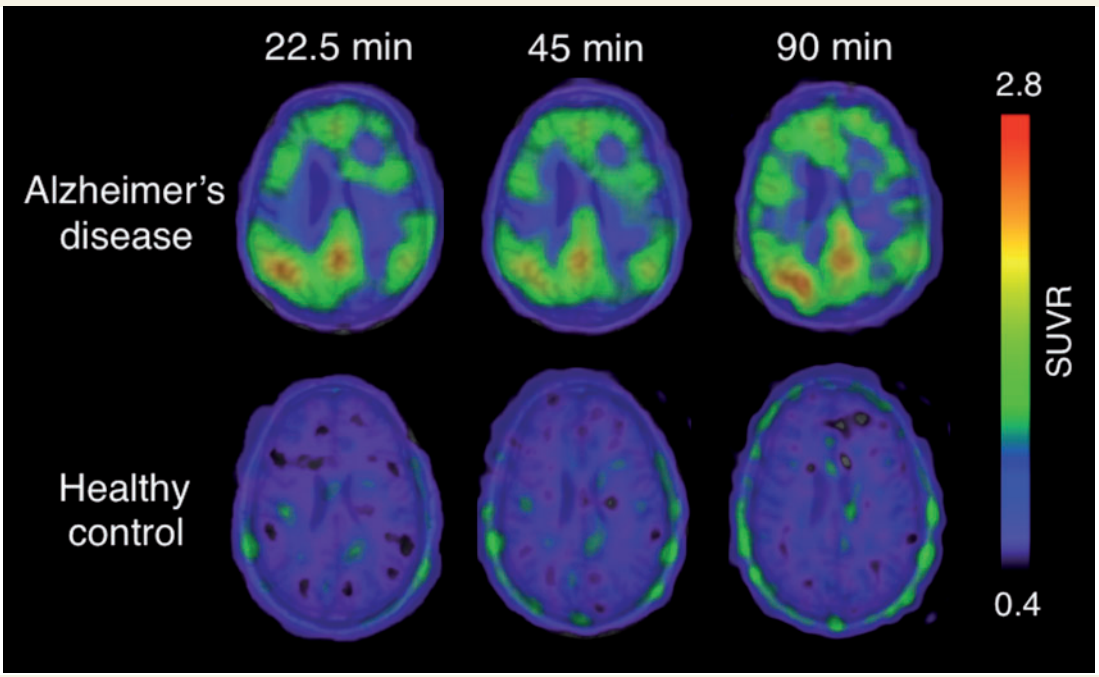

Figure 5 ^{123}I-ABC577 SPECT images of different scan lengths. Comparison of axial SPECT images of different scan lengths (22.5, 45, and 90 min) at constant scan start time (150 min for Alzheimer's disease and 120 min for healthy control) for one representative patient with Alzheimer's disease (AD01) and one healthy control subject (HC01). SPECT images are overlaid on individual coregistered magnetic resonance images.

Table 2 Regional SUVR values of ^{123}I-ABC577 and ^{18}F-florbetapir

Region	^{123}I-ABC577		^{18}F-florbetapir
	Healthy controls (n = 3)	Alzheimer's disease (n = 3)	Alzheimer's disease (n = 3)
Frontal cortex	0.74 ± 0.03	1.22 ± 0.32	1.29 ± 0.13
Parietal cortex	0.77 ± 0.03	1.23 ± 0.26	1.37 ± 0.21
Temporal cortex	0.85 ± 0.07	1.39 ± 0.32	1.32 ± 0.15
Occipital cortex	0.83 ± 0.10	1.01 ± 0.11	1.12 ± 0.25
Anterior cingulate	0.78 ± 0.05	1.28 ± 0.30	1.28 ± 0.05
Posterior cingulate	0.84 ± 0.04	1.40 ± 0.22	1.48 ± 0.11
Subcortical white matter	0.80 ± 0.01	0.98 ± 0.09	1.62 ± 0.16
Cortical average	0.80 ± 0.04	1.26 ± 0.25	1.31 ± 0.10

Data are expressed as mean ± standard deviation.

patients with Alzheimer's disease relative to control subjects. The difference in tracer retention in the cortical areas between Alzheimer's disease and healthy controls was highest in the posterior cingulate (mean ± SD, 1.40 ± 0.22 versus 0.84 ± 0.04) and lowest in the occipital cortex (mean ± SD, 1.01 ± 0.11 versus 0.83 ± 0.10). The mean cortical-to-cerebellar SUVR values were 1.26 ± 0.25 and 0.80 ± 0.04 for patients with Alzheimer's disease and healthy control subjects, respectively.

Average SUVR values and PET images for 15 min of acquisitions with ^{18}F-florbetapir are shown in Table 2 and Fig. 6. As reported previously, accumulation of ^{18}F-florbetapir can be seen in the cortical regions. Both cortical binding of ^{123}I-ABC577 and that of ^{18}F-florbetapir were greater in the posterior cingulate and temporal cortex, and lesser in the occipital cortex. The white matter binding of ^{123}I-ABC577 was lower than that of ^{18}F-florbetapir. The SUVR values for the white matter in the same Alzheimer's disease subjects were 0.98 ± 0.09 and 1.62 ± 0.16 for ^{123}I-ABC577 and ^{18}F-florbetapir, respectively.

Discussion

The aim of the current research programme is to develop an amyloid-β imaging tracer for SPECT that is comparable in performance to PET tracers. Because of the lower operating cost and wider accessibility of SPECT relative to PET, SPECT is better suited for routine clinical use and primary screening for subjects with preclinical Alzheimer's disease (Sperling *et al.*, 2011). Given that the number of patients with Alzheimer's disease is expected to increase dramatically worldwide (Ferri *et al.*, 2005; Prince *et al.*, 2013), the development of a useful amyloid-β imaging agent for SPECT is a critical issue for society. To date, ^{123}I-2-(4′-dimethylaminophenyl)-6-iodo-imidazo[1,2-a]pyridine (^{123}I-IMPY) is the only tracer for SPECT that has been tested in humans (Newberg *et al.*, 2006). However, the preliminary clinical data showed that the target-to-background ratio of ^{123}I-IMPY for amyloid-β plaque labelling was not as robust as that of PET tracers, making it difficult to

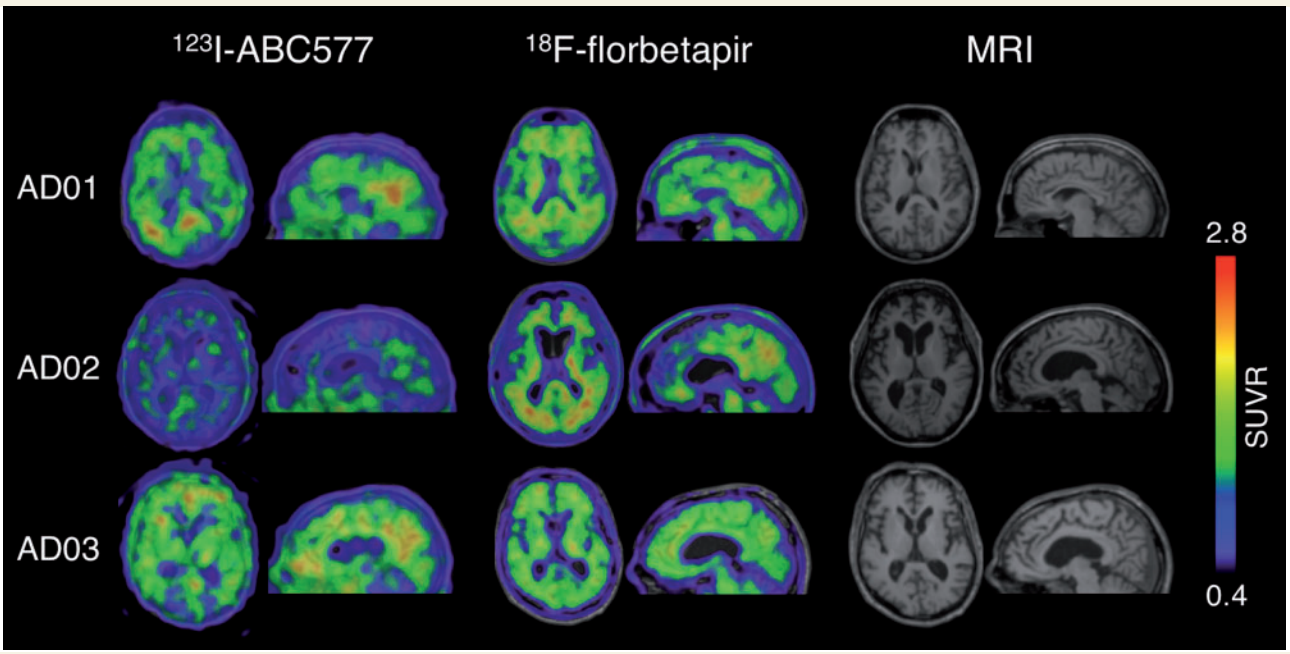

Figure 6 Comparison of ^{123}I-ABC577 and ^{18}F-florbetapir. ^{123}I-ABC577 SPECT images from 150–240 min post-injection (*left*) and ^{18}F-florbetapir PET images from 50–65 min post-injection (*middle*) in the patients with Alzheimer's disease. Co-registered magnetic resonance images are shown on the *right*. Axial views include the frontal lobe, anterior cingulate, posterior cingulate, insula, striatum, and lateral temporal lobe. Sagittal views include the anterior cingulate, posterior cingulate, and precuneus.

distinguish healthy controls from patients with Alzheimer's disease (Kung *et al.*, 2012). Thus, there is no SPECT imaging probe available for the clinical diagnosis of Alzheimer's disease. In this study, we first evaluated the biological potential of novel SPECT agent ^{123}I-ABC577 in preclinical settings. In addition, its suitability as an imaging agent for amyloid-β in the brain was examined in a SPECT study of healthy controls and Alzheimer's disease patients. The present findings demonstrate the feasibility of non-invasive determination of amyloid-β plaques in human subjects with ^{123}I-ABC577.

In the binding assays, unfixed frozen post-mortem human brain tissues were chosen for the saturation binding study and *in vitro* autoradiography for accurate prediction of *in vivo* binding performance in humans. ^{123}I-ABC577 displayed high binding affinity to homogenate prepared from the grey matter of an Alzheimer's disease patient. The K_d value of ^{123}I-ABC577 (1.8 nM) is very close to that of known amyloid-β imaging agents, such as ^{18}F-florbetapir (3.7 nM; Choi *et al.*, 2009) and ^{11}C-Pittsburgh compound B (1.4 nM; Mathis *et al.*, 2003), indicating that ^{123}I-ABC577 has enough binding affinity for amyloid-β to use in clinical tests. *In vitro* autoradiography studies in combination with immunohistochemistry provide support for the view that ^{123}I-ABC577 selectively binds to amyloid-β. In the hippocampal section examined, the distribution of ^{123}I-ABC577 co-localized with amyloid-β immunostaining of plaques but not with tau pathology. The off-target binding profiles were assessed further using ABC577 against various receptors, ion channels, and transporters, and no remarkable inhibition was observed at the high concentration of 10 μM.

The ability to penetrate the intact blood–brain barrier is an essential factor in the success of an imaging agent for amyloid-β plaques in the brain (Mathis *et al.*, 2012). In biodistribution studies, ^{123}I-ABC577 demonstrated not only high initial brain uptake but also good clearance from the normal rat brain. Because no amyloid-β plaques are expected in the healthy rat brain, the washout of tracer from the brain should be rapid to yield a higher signal-to-noise ratio earlier in the Alzheimer's disease brain.

Because SPECT is inferior to PET in terms of sensitivity and quantitative performance, SPECT radiotracers should be more sensitive and selective than PET tracers to amyloid-β plaques. Our initial preclinical characterization demonstrated that ^{123}I-ABC577 has promising properties with a high binding affinity and selectivity for amyloid-β plaques, as well as favourable brain kinetics in the healthy rat brain.

In the clinical study, ^{123}I-ABC577 enabled a clear distinction between patients with Alzheimer's disease and healthy controls. This distinction was apparent via visual assessment or a simple quantitative measure, the ratio of cortical-to-cerebellar binding. The current results suggest that, when applied after 150 min, scans as short as 22.5–45 min could be sufficient to discriminate between Alzheimer's disease patients and healthy controls (Fig. 5). In the present study, the SPECT images were obtained only

from 150 min to 240 min post-injection; therefore, the optimal timing of scan initiation should be determined in a future study.

In healthy controls, there was no evident difference in radioactivity between cortical regions and the cerebellum. On the other hand, in patients with Alzheimer's disease, ^{123}I-ABC577 demonstrated prominent accumulation in grey matter cortical areas, such as the frontal cortex, temporal cortex, and posterior cingulate, and less accumulation in the occipital cortex. The cortical binding pattern of ^{123}I-ABC577 is relatively similar to that of ^{18}F-florbetapir in the same Alzheimer's disease subjects, and this pattern is consistent with the known localization of amyloid-β plaques (Braak and Braak, 1991) and with results from other amyloid-β radiotracers (Rowe *et al.*, 2007, 2008; Nyberg *et al.*, 2009). Taken together with the results of the *in vitro* ^{123}I-ABC577 binding studies, the present *in vivo* observations suggest that ^{123}I-ABC577 binds specifically to amyloid-β plaques.

The mean cortical-to-cerebellar SUVR for ^{123}I-ABC577 in Alzheimer's disease patients was 58% greater than in healthy controls. It has been reported that the mean cortical-to-cerebellar SUVR for ^{18}F-florbetapir were 1.42 ± 0.24 and 1.00 ± 0.05 for Alzheimer's disease patients and healthy controls (age: <55 years), respectively, indicating a 42% greater SUVR in Alzheimer's disease patients relative to healthy controls (Joshi *et al.*, 2012). Although it is difficult to directly compare the present with previous findings because of differences in resolution, study population, and evaluation methods, the present result indicates that ^{123}I-ABC577 has the potential to provide images in which the contrast between healthy controls and Alzheimer's disease patients is comparable to that yielded by PET tracers.

Although amyloid-β imaging radiotracers for PET that have been approved for clinical use show high non-specific binding in the white matter (Rowe and Villemagne, 2013), no significant white matter uptake was observed on the ^{123}I-ABC577 images. In healthy controls, there was no evident difference between binding in the grey and white matter (Fig. 4 and Table 2). In patients with Alzheimer's disease, ^{123}I-ABC577 clearly demonstrated high radiotracer binding in extensive areas of the grey matter compared to the white matter region. On the other hand, ^{18}F-florbetapir showed a non-specific white matter binding that was similar to, rather than greater than, cortical binding in the same Alzheimer's disease subjects (Fig. 6 and Table 2). The lower white matter signal for ^{123}I-ABC577 might have been partly due to the rapid metabolism of ^{123}I-ABC577 in plasma, as well as low non-specific binding, as shown in the preclinical analyses. The relatively low background radioactivity indicates that ^{123}I-ABC577 images may yield easier and more reliable assessment in clinical practice than the currently available PET tracers.

Because this was the first human study designed to evaluate the potential of ^{123}I-ABC577, the sample size was relatively small and we were unable to perform any statistical analysis. Furthermore, to compare specific ^{123}I-ABC577 binding in Alzheimer's disease patients with the lack of specific binding in controls, young healthy controls were enrolled instead of age-matched control subjects. Further large studies involving age-matched controls are required to validate the preliminary findings of the present study and to optimize both the imaging protocol and the quantification method.

In summary, we successfully designed and synthesized a novel SPECT amyloid-β imaging agent with a high affinity for amyloid-β and desirable brain pharmacokinetics. In the first such clinical study, ^{123}I-ABC577 demonstrated a favourable safety profile and a good ability to differentiate Alzheimer's disease patients from healthy controls. No conspicuous accumulation of radioactivity was observed in the white matter. These preliminary data suggest that ^{123}I-ABC577 may be a useful SPECT imaging tool to identify amyloid-β in the human brain. The availability of a SPECT amyloid-β tracer may provide increased accessibility to an imaging diagnostic tool for Alzheimer's disease.

Acknowledgements

The authors would like to thank Chihiro Usui, Tadashi Iwasaki, and Yukie Tomizawa for their assistance with this study.

Funding

This study was supported by Nihon Medi-Physics Co., Ltd.

Supplementary material

Supplementary material is available at *Brain* online.

References

Aisen PS, Petersen RC, Donohue MC, Gamst A, Raman R, Thomas RG, et al. Clinical core of the Alzheimer's Disease neuroimaging initiative: progress and plans. Alzheimer's Dement 2010; 6: 239–46.

Barthel H, Gertz HJ, Dresel S, Peters O, Bartenstein P, Buerger K, et al. Cerebral amyloid-beta PET with florbetaben (^{18}F) in patients with Alzheimer's disease and healthy controls: a multicentre phase 2 diagnostic study. Lancet Neurol 2011; 10: 424–35.

Bateman RJ, Xiong C, Benzinger TL, Fagan AM, Goate A, Fox NC, et al. Clinical and biomarker changes in dominantly inherited Alzheimer's disease. N Engl J Med 2012; 367: 795–804.

Braak H, Braak E. Neuropathological stageing of Alzheimer-related changes. Acta Neuropathol 1991; 82: 239–59.

Chen CJ, Bando K, Ashino H, Taguchi K, Shiraishi H, Shima K, et al. *In vivo* SPECT Imaging of Amyloid-beta Deposition with Radioiodinated Imidazo[1,2-a]Pyridine Derivative DRM106 in a Mouse Model of Alzheimer's Disease. J Nucl Med 2015; 56: 120–6.

Choi SR, Golding G, Zhuang Z, Zhang W, Lim N, Hefti F, et al. Preclinical properties of ^{18}F-AV-45: a PET agent for Abeta plaques in the brain. J Nucl Med 2009; 50: 1887–94.

Clark CM, Schneider JA, Bedell BJ, Beach TG, Bilker WB, Mintun MA, et al. Use of florbetapir-PET for imaging beta-amyloid pathology. JAMA 2011; 305: 275–83.

Ferri CP, Prince M, Brayne C, Brodaty H, Fratiglioni L, Ganguli M, et al. Global prevalence of dementia: a Delphi consensus study. Lancet 2005; 366: 2112–7.

Hardy JA, Higgins GA. Alzheimer's disease: the amyloid cascade hypothesis. Science 1992; 256: 184–5.

Huijbers W, Mormino EC, Schultz AP, Wigman S, Ward AM, Larvie M, et al. Amyloid-beta deposition in mild cognitive impairment is associated with increased hippocampal activity, atrophy and clinical progression. Brain 2015; 138 (Pt 4): 1023–35.

Joshi AD, Pontecorvo MJ, Clark CM, Carpenter AP, Jennings DL, Sadowsky CH, et al. Performance characteristics of amyloid PET with florbetapir F 18 in patients with Alzheimer's disease and cognitively normal subjects. J Nucl Med 2012; 53: 378–84.

Kung HF, Kung MP, Zhuang ZP, Hou C, Lee CW, Plossl K, et al. Iodinated tracers for imaging amyloid plaques in the brain. Mol Imaging Biol 2003; 5: 418–26.

Kung MP, Weng CC, Lin KJ, Hsiao IT, Yen TC, Wey SP. Amyloid plaque imaging from IMPY/SPECT to AV-45/PET. Chang Gung Med J 2012; 35: 211–8.

Mathis CA, Mason NS, Lopresti BJ, Klunk WE. Development of positron emission tomography beta-amyloid plaque imaging agents. Semin Nucl Med 2012; 42: 423–32.

Mathis CA, Wang Y, Holt DP, Huang GF, Debnath ML, Klunk WE. Synthesis and evaluation of ^{11}C-labeled 6-substituted 2-arylbenzothiazoles as amyloid imaging agents. J Med Chem 2003; 46: 2740–54.

McKhann GM, Knopman DS, Chertkow H, Hyman BT, Jack CR, Jr., Kawas CH, et al. The diagnosis of dementia due to Alzheimer's disease: recommendations from the National Institute on Aging-Alzheimer's Association workgroups on diagnostic guidelines for Alzheimer's disease. Alzheimer's Dement 2011; 7: 263–9.

Mintun MA, Larossa GN, Sheline YI, Dence CS, Lee SY, Mach RH, et al. [^{11}C]PIB in a nondemented population: potential antecedent marker of Alzheimer disease. Neurology 2006; 67: 446–52.

Nelissen N, Van Laere K, Thurfjell L, Owenius R, Vandenbulcke M, Koole M, et al. Phase 1 study of the Pittsburgh compound B derivative ^{18}F-flutemetamol in healthy volunteers and patients with probable Alzheimer disease. J Nucl Med 2009; 50: 1251–9.

Newberg AB, Wintering NA, Plossl K, Hochold J, Stabin MG, Watson M, et al. Safety, biodistribution, and dosimetry of ^{123}I-IMPY: A novel amyloid plaque-imaging agent for the diagnosis of Alzheimer's disease. J Nucl Med 2006; 47: 748–54.

Nyberg S, Jonhagen ME, Cselenyi Z, Halldin C, Julin P, Olsson H, et al. Detection of amyloid in Alzheimer's disease with positron emission tomography using [^{11}C]AZD2184. Eur J Nucl Med Mol Imaging 2009; 36: 1859–63.

Ono M, Cheng Y, Kimura H, Watanabe H, Matsumura K, Yoshimura M, et al. Development of novel ^{123}I-labeled pyridyl benzofuran derivatives for SPECT imaging of beta-amyloid plaques in Alzheimer's disease. PLoS One 2013; 8: e74104.

Prince M, Bryce R, Albanese E, Wimo A, Ribeiro W, Ferri CP. The global prevalence of dementia: a systematic review and metaanalysis. Alzheimer's Dement 2013; 9: 63–75, e2.

Qu W, Kung MP, Hou C, Benedum TE, Kung HF. Novel styrylpyridines as probes for SPECT imaging of amyloid plaques. J Med Chem 2007; 50: 2157–65.

Reiman EM, Langbaum JB, Fleisher AS, Caselli RJ, Chen K, Ayutyanont N, et al. Alzheimer's Prevention Initiative: a plan to accelerate the evaluation of presymptomatic treatments. J Alzheimer's Dis 2011; 26 (Suppl 3): 321–9.

Roberson ED, Mucke L. 100 years and counting: prospects for defeating Alzheimer's disease. Science 2006; 314: 781–4.

Rowe CC, Ackerman U, Browne W, Mulligan R, Pike KL, O'Keefe G, et al. Imaging of amyloid beta in Alzheimer's disease with ^{18}F-BAY94-9172, a novel PET tracer: proof of mechanism. Lancet Neurol 2008; 7: 129–35.

Rowe CC, Ng S, Ackermann U, Gong SJ, Pike K, Savage G, et al. Imaging beta-amyloid burden in aging and dementia. Neurology 2007; 68: 1718–25.

Rowe CC, Villemagne VL. Brain amyloid imaging. J Nucl Med Technol 2013; 41: 11–8.

Schneider LS, Mangialasche F, Andreasen N, Feldman H, Giacobini E, Jones R, et al. Clinical trials and late-stage drug development for Alzheimer's disease: an appraisal from 1984 to 2014. J Intern Med 2014; 275: 251–83.

Sperling RA, Mormino E, Johnson K. The evolution of preclinical Alzheimer's disease: implications for prevention trials. Neuron 2014; 84: 608–22.

Sperling RA, Aisen PS, Beckett LA, Bennett DA, Craft S, Fagan AM, et al. Toward defining the preclinical stages of Alzheimer's disease: recommendations from the National Institute on Aging-Alzheimer's Association workgroups on diagnostic guidelines for Alzheimer's disease. Alzheimer's Dement 2011; 7: 280–92.

Sperling RA, Laviolette PS, O'Keefe K, O'Brien J, Rentz DM, Pihlajamaki M, et al. Amyloid deposition is associated with impaired default network function in older persons without dementia. Neuron 2009; 63: 178–88.

Vandenberghe R, Van Laere K, Ivanoiu A, Salmon E, Bastin C, Triau E, et al. ^{18}F-flutemetamol amyloid imaging in Alzheimer disease and mild cognitive impairment: a phase 2 trial. Ann Neurol 2010; 68: 319–29.

Villemagne VL, Burnham S, Bourgeat P, Brown B, Ellis KA, Salvado O, et al. Amyloid beta deposition, neurodegeneration, and cognitive decline in sporadic Alzheimer's disease: a prospective cohort study. Lancet Neurol 2013; 12: 357–67.